Atmos. Chem. Phys. Discuss., 10, 24345–24370, 2010
www.atmos-chem-phys-discuss.net/10/24345/2010/
doi:10.5194/acpd-10-24345-2010

Atmospheric Chemistry and Physics Discussions

Numerical modelling of microburst with Large-Eddy Simulation

V. Anabor[1], U. Rizza[2,1], G. A. Degrazia[1], and E. de Lima Nascimento[1]

[1]Departamento de Fisica, Universidade Federal de Santa Maria, Santa Maria, RS, Brasil
[2] Institute of Atmospheric Sciences and Climate, CNR/ISAC, Lecce, Italy

Received: 15 September 2010 – Accepted: 6 October 2010 – Published: 20 October 2010

Correspondence to: U. Rizza (u.rizza@isac.cnr.it)

Published by Copernicus Publications on behalf of the European Geosciences Union.

Abstract

An isolated and stationary microburst is simulated using a 3-D time-dependent, high resolution Large-Eddy Simulation (LES) model. The microburst downdraft is initiated by specifying a simplified cooling source at the top of the domain near 2 km. The modelled time scale for this damaging wind (30 m/s) is of order of few min with a spatial scale enclosing a region with 500 m radius around the impact point. These features are comparable with results obtained from full-cloud models. The simulated flow shows the principal features observed by Doppler radar and others observational full-scale downburst events. In particular are observed the expansion of the primary and secondary cores, the presence of the ring vortex at the leading edge of the cool outflow, and finally an accelerating outburst of surface winds.

This result evidences the capability of LES to reproduce complexes phenomena like a Microburst and indicates the potential of LES for utilization in atmospheric phenomena situated below the storm scale and above the microscale, which generally involves high velocities in a short time scale.

1 Introduction

During the life cycle of a thunderstorm, complex circulations are developed. During its developing stage the storm structure is dominated by low-level convergence and deep and intense updrafts that transport moisture and warm air from the environmental boundary layer to the storm. As precipitation forms, negative buoyancy is generated due to evaporation of raindrops in contact with entrained air (or the melting of hydrometeors). At this stage stronger downdrafts are formed while updrafts are weakened. On some occasions the cooled air becomes so negatively buoyant that intense downdrafts are generated inducing strong winds at ground level. This physical mechanism can lead to the formation of downbursts (Fujita, 1985).

ACPD

10, 24345–24370, 2010

Fujita (1985) defines a downburst as a short-lived strong downdraft that induces a highly divergent outburst. These damaging winds can be either straight or curved. A microburst is defined as a small-scale downburst with its outburst and winds extending for only 4 km or less. In spite of its small horizontal scale, an intense microburst could induce damaging winds as high as 75 m/s (270 km/h). For such reasons microbursts can be specially dangerous to aircraft during takeoff and landing due to the intense wind shear accompanying them (Elmore et al., 1986). Microbursts have been the subject of several observational and numerical studies since the pioneering works of Fujita (1975). Field studies such as JAWS (McCarthy et al., 1982), NIMROD (Fujita, 1979) and FLOWS (Wolfson et al., 1986) have sampled hundreds of microbursts with single/multiple Doppler radar data. These field studies allowed a better understanding of the physical properties of microbursts, and helped foster the development of numerical models that simulate microburst-producing storms.

Generally, numerical models employed to study microbursts fall into two main categories: sub-cloud models and full cloud microburst models (Orf and Anderson, 1999). In the former category some sort of forcing – representing the bulk effect of microphysical processes that generate negative buoyancy in a storm – is usually imposed in the upper portion of the model domain (Anderson et al., 1992; Orf et al., 1996); in the latter category the full life cycle of the microburst-producing storm is modelled (Hjelmfelt et al., 1989; Proctor, 1989; Straka and Anderson, 1993). In an attempt to model the microburst phenomenon Srivastava (1985, 1987) used simple one-dimensional time dependent models of strong downdrafts forced by evaporative cooling and melting precipitation. Orf and Anderson (1999) used a k-ε model to investigate the effects of travelling microbursts in unidirectional sheared environments. In the context of sub-cloud modelling of microbursts with engineering applications some recent studies include that of Nicholls et al. (1993), which performed a 2-D Large-Eddy Simulation of a microburst on a building model. Kim and Hangan (2007) used the CFD software Fluent 6.0 (FLUENT, 2001) in a 2-D setup to investigate the macro-scale flow dynamics of an impinging jet. Sengupta et al., 2001 performed both experimental and numerical simulations of

ACPD
10, 24345–24370, 2010

microburst winds, while Mason et al. (2009) developed a dry 2-D non-hydrostatic model implemented within the CFD commercial code ANSYS CFX11 (ANSYS, 2007).

Sub-cloud modelling of microbursts not including cloud microphysics nor large scale atmospheric processes can be performed at very high resolution, allowing the analysis of detailed structure of the near-ground flow dynamics, where the highest wind speeds are usually detected during microbursts. The thermal forcing for these simulations is usually parameterized using a spatio-temporal variable function that is decoupled from microphysics and moisture advection (Orf et al., 1996).

In the present study the microburst dynamics is investigated using a Large-Eddy Simulation (LES) model that has been largely employed by the scientific community to study the properties of planetary boundary layer (PBL) flows. LES is a well-established technique to study the 3-D turbulent characteristics of PBL, as vastly documented in the literature (Lesieur and Métais, 1996). Nevertheless, the number of LES studies addressing sub-cloud microburst modelling is still scarce mainly due to the required high computational cost. More recently the availability of less expensive platforms for parallel computing has made the LES strategy more appealing and not so prohibitive as in the past.

The aim of this study is to test the ability of LES in reproducing the intense downward wind currents associated with a microburst. This will be accomplished with idealised conditions typical of sub-cloud modelling in which the cooling forcing that generates the microburst is parameterized following Orf et al. (1996).

2 Mechanism driving microburst

A microburst event has its physical origin in the microphysical and thermodynamic process of a convective cloud (Mahoney and Rodi, 1987). These processes are explored by Srivastava (1985, 1987) using a simple one-dimensional time-dependent model of an evaporatively and melting precipitation driven downdraft. The downdraft intensity increases as the lapse rate in the environment and rainwater mixing ratio increases,

ACPD
10, 24345–24370, 2010

and as the raindrop size decreases (Srivastava, 1985). When the lapse rate of environmental temperature approaches the dry-adiabatic profile, even very light precipitation can drive intense downdrafts. As thermal stratification and stability increases, progressively higher cloud water content (liquid and ice) is needed to produce intense downdrafts (Srivastava, 1987). A very favourable microburst environment should present a dry-adiabatic like sub-cloud temperature profile (Wakimoto, 1985), high concentration of small hydrometeors (ice or liquid) melting or evaporating (Wakimoto, 1985, 1994).

Atlas et al. (2004) analysed a unique set of Doppler and polarimetric radar observations of a microburst-producing storm during Tropical Rainfall Measuring Mission (TRMM) Large-Scale Biosphere-Atmosphere (LBA) field experiment. The results closely matched with the initial conditions and results of Srivastava (1985, 1987). This suggests that only modest size hail in large concentrations that melt aloft can produce wet microbursts. The narrower the distribution of hail particle sizes, the more confined will be the layer of melting and negative buoyancy, and the more intense the microburst.

The downdraft acceleration can be schematically represented by the vertical component of the equation of motion (Houze, 1993).

$$\frac{Dw}{Dt} = -\frac{1}{\rho_0}\frac{\partial p^*}{\partial z} + B(\theta_v^*, p^*, \mathrm{qH}) \quad (1)$$

Where w is the vertical velocity, p^* is the pressure perturbation from the basic state, and B is the buoyancy term which depends on virtual temperature (θ_v^*), pressure (p^*) and hydrometeor loading (qH). As the pressure gradient force is usually small compared with the buoyancy in the storm scale (Bluestein, 1993), the buoyancy term contains the most important part of the microburst producing phenomena.

3 Model description

To perform the sub-cloud modelling of a microburst, we adapted the Large-Eddy Simulation code of Moeng (1984). The code version chosen is the dry one, such that no

ACPD
10, 24345–24370, 2010

microphysical parameterisation is needed. The complete derivation of the resolved scale equations can be found in Moeng (1984) and Sullivan et al. (1994).

Only the equations that are relevant to the understanding of the microburst dynamics are discussed here. In our simulations the negative buoyancy that drives the microburst formation is parameterised by imposing an additional source term *Q(x,y,z;t)* in the equation for the virtual potential temperature, as follows:

$$\frac{\partial \bar{\theta}}{\partial t} = -\bar{u}_j \frac{\partial \bar{\theta}}{\partial x_j} - \frac{\partial \tau_{\theta j}}{\partial x_j} + Q(x,y,z;t) \quad (2)$$

where $\bar{\theta}$ is the resolved virtual potential temperature field, $(\bar{u}_1, \bar{u}_2, \bar{u}_3) \equiv (\bar{u}, \bar{v}, \bar{w})$ is the resolved velocity field and $\tau_{\theta j}$ is the tensor that represents the subgrid closure for the temperature field. The boundary conditions in the horizontal were periodic, the upper boundary was specified as a frictionless rigid lid with zero mass, momentum, heat and subgrid kinetic energy flux, and the bottom boundary employed a no-slip condition with a prescribed roughness length.

The use of a cooling function, in the context of subcloud modelling, avoids the use of explicit microphysics routines, which are computationally very expensive. Furthermore the shape, duration and amplitude parameters of the cooling function may be easily chosen providing an easier interpretation of the modelling results.

4 Methodology

The main driving mechanism for the downburst is given by the buoyancy term in eq.1 that represents physical processes such as cooling due to melting and evaporation of hydrometeors.

In the LES configuration a cooling function parameterising the bulk effect of these processes is placed at the top the domain, near 2 km.

ACPD
10, 24345–24370, 2010

In the sub-cloud LES model used here the spatial-temporal cooling function is parameterised using the approach of Orf et al. (1996), that is:

$$Q(x,y,z;t) = \begin{cases} g(t)\cos^2(\pi R) \text{ for } R < 1/2 \\ 0 \text{ for } R > 1/2 \end{cases}$$

where R is the normalised distance from the centre of cooling, given by

$$R = \sqrt{\left(\frac{x-x_f}{M_x}\right)^2 + \left(\frac{y-y_f}{M_y}\right)^2 + \left(\frac{z-z_f}{M_z}\right)^2}$$

where (x_f, y_f, z_f) is the location of the center of the forcing function and (M_x, M_y, M_z) is its horizontal/vertical extension (Table 1).

The variable $g(t)$ is the time modulation of the magnitude of the forcing function that follows Orf et al. (1996), being described by:

$$\begin{cases} g(t) = \cos^2(\frac{\pi t}{2\tau}) & 0 \le t < 120 \quad \text{and} \quad 720 < t \le 840 \\ g(t) = -1 & 120 \le t \le 720 \end{cases}$$

where $\tau = 120$ s. This means that it ramps to a maximum value after 2 min, after which a constant value is kept for 10 min, followed by a gradual decrease in the last 2 min as depicted in Fig. 1. An intense source as employed in Mason et al. (2009) has been used here, with a maximum cooling rate of −0.08 K/s to produce a more intense downburst event.

Dry microbursts typically occur in a sub-cloud environment with a deep dry adiabatic profile (that might extend up to 2 km a.g.l. or higher, Wakimoto, 1985), which is indicative of a PBL in dry neutral conditions.

In this context, LES is the adequate numerical tool to simulate a neutral PBL (Andren et al., 1994). By varying the geostrophic wind and the surface heat flux, different turbulent regimes can be generated with LES. A "prototype" of a neutral PBL may be

ACPD
10, 24345–24370, 2010

obtained by first generating a convective PBL by imposing an upward heat flux, followed by a gradual weakening of the heat flux, allowing a quick spin-up to a steady shear flow (Moeng and Sullivan, 1994).

In the present work, simulations were performed in a 10 × 10 km horizontal rectangular domain that is 2 km deep with 128^3 grid points. The convective simulation started from a barotropic condition, that is, with the geostrophic wind constant throughout the numerical domain. Internal parameters such as the extension of domain, grid size, geostrophic winds, kinematic surface heat flux (Q_*), and initial capping inversion height $(z_i)_0$ are summarised in Table 2. After reaching a steady state Convective Boundary Layer (CBL) the heat flux was turned off and a neutral PBL was simulated for the following 6 h. In Fig. 2 are shown the mean wind and temperature profile snapshots taken at the end of the convective simulation (CON) and at the end of neutral simulation (NEU). It should be noticed that profiles of "sheared" wind speed is attained as a consequence of the surface frictional stresses. Meanwhile the constant potential temperature profile, typical of a neutral PBL conditions is evident in Fig. 2.

The cooling forcing function is activated exactly at the end of the neutral simulation. According to the imposed time modulation of the forcing function (Fig. 1) the forcing lasted for 14 min and covered an area of (2,2) km in the upper region of the simulation domain.

5 Results and discussion

5.1 Qualitative comparisons

In the case of an isolated static microburst, the main features to note are the downdraft core, wall jet and the roll vortices (Orf et al., 1996). The term "wall jet" is usually employed in fluid dynamics to illustrate the typology of shallow flow that occurs when a cold fluid impinges a flat surface at high speed (Hjelmfelt, 1988).

ACPD
10, 24345–24370, 2010

The cooling function applied at the top of the domain generates a downdraft with vertical velocity reaching approximately 20 m/s. Just after the impact with the ground a cold high pressure dome is generated around the impact point. The induced pressure gradient force across the pressure dome transfers the momentum associated with the impinging downdraft to a cold outflow current. This leads to the development of a divergent wall jet, corresponding to the highest wind speeds generated in this simulation.

At the leading edge of the wall jet there is a strong horizontal gradient in buoyancy that leads to the development of horizontal vorticity, which is manifested as a vortex ring circulation. The wall jet, as a negatively buoyant downdraft, maintains and expands the vortex ring circulation. The sequence of Fig. 3a–e depicts the magnitude of surface winds speeds at the first vertical level of the LES grid, respectively 3, 5, 6, 8 and 10 min into the simulation. The general picture that may be understood examining Fig. 3a–e is the following: around the impact point, just a few seconds after the cold plume impinges on the surface a "primary" core is developed (Fig. 3a, b). The highest surface speeds are generated during this stage for the reasons explained above.

The expansion of this "primary" core is maintained by the strong horizontal pressure gradient. As the "primary" core expands, the effect of surface friction and turbulent mixing reduces the pressure gradient at its leading edge (Fig. 3c). This process evolves in a time scale on the order of 1 min.

In the meantime, the cold downdraft continues impinging on the surface forming a "secondary" core (Fig. 3d). The turbulent mixing generated by the passage of the primary outflow reduces the horizontal pressure gradient force resulting in non-expansion of the secondary core (Fig. 3e). Accordingly the horizontal buoyancy gradient is also weakened, such that the generation of horizontal vorticity due to baroclinic effect is reduced, avoiding the formation of a secondary vortex ring.

The reproduction of a neutral PBL that is typical of the microburst environment has as effect the presence of a predominant longitudinal mean wind ($\sim 3\,\mathrm{ms}^{-1}$) and a weak lateral component ($\sim 0.3\,\mathrm{ms}^{-1}$). During the microburst development it is possible to identify latitudinal symmetry (Fig. 3c) and longitudinal asymmetry along the vortex ring

ACPD
10, 24345–24370, 2010

(Figs. 3c and 4a, b, c).

This asymmetry is the result of the predominant wind (u component) interaction with the vertical velocity in the microburst plume. Figure 4a shows a mean flow channelling into the cold microburst. Figure 4b depicts the evidence of the vortex ring development along the upwind side of the microburst as a result of the interaction between the mean flow and the microburst surface upstream currents. Along the downwind side of the microburst the vortex ring is generated a few minutes later, since the microburst outflow has the same direction of the mean flow (Fig. 4b, c).

Figure 5 shows the vertical distribution of the maximum radial velocity. The radial velocity is calculated from the centre of the numerical domain, at each radial distance with a bilinear interpolation of the resolved horizontal components ($\bar{u}, \bar{v}$) in the eight closest points of the LES grid. Notice that the maximum velocity of the impinging jet, after 84 s is located at about 1000 meters above ground level (m a.g.l.) with a speed of 8 m/s. This is possibly caused by the horizontal divergence induced by the passage of the cold downdraft at that level. After 135 s the maximum (10 m/s) is located about 600 m a.g.l.; after 174 s it is located at 150 m a.g.l. and the speed is close to 15 m/s. After the impact the surface velocity increase rapidly reaching 35 m/s in almost one minute. This picture shows that the radial velocity is growing and displacing downward following the edge of the cold plume. This is also in agreement with the classic "picture" describing a microburst as characterized by strong localized downflow and an outburst of strong winds near the surface.

The time-radial distance plot (Fig. 6) shows the surface wind speeds ($M = (\bar{u}^2 + \bar{v}^2)^{1/2}$) and spatial structure of the magnitude of the wind field at the first vertical level of the LES grid. A remarkable feature is evident: the primary core forms 4–5 min after the start of cooling with highest speeds ($\sim 30\,\mathrm{ms}^{-1}$) occurring in the first 500 m, and decreasing radially from the microburst centre. The vortex ring is present at the leading edge of the core expansion and travels for about 2000 m in less than 5 min. The secondary core appears two min after the formation of first core ($\sim$6 min) with lower speeds ($\sim 20\,\mathrm{ms}^{-1}$) and smaller expansion ($\sim$1500 m).

ACPD
10, 24345–24370, 2010

There is a reduction of the horizontal pressure gradient after the passage of the primary vortex ring. Therefore, smaller wind speeds are observed during the secondary core expansion. During the radial expansion is possible to notice the kinetic energy dissipation (Fig. 6).

A quasi-periodic (~2 min) oscillation is present in the time-radial plot of the wind speed. It is an evidence that the conversion of the downward kinetic energy into horizontal kinetic energy does not occur continually, but as a sequence of outbursts. Because the model applies the incompressibility condition that filters out acoustic waves, this oscillation may be a manifestation of internal gravity waves. This results in a fast increasing horizontal pressure gradient, followed by an outward horizontal acceleration of the flow. The time to build up this potential energy is about 2 min that is observed by the quasi-periodic behaviour of the wind magnitude close to the microburst center (first 500 m).

Doppler radar observations show that a microburst is characterized when the downward current hits the ground generating a strong divergence at its center, such that an accelerated outburst of surface winds can be observed. This simulation close reproduces the Doppler Radar observations and highlights the LES capability to reproduce complex thermal and dynamical phenomena like microbursts, jet streaks and other events involving high velocities.

5.2 Quantitative comparison

The maximum simulated storm event wind speed U_{storm} (Mason et al., 2009) was 38.4 m/s at the first LES vertical level (≈16 m) four min after the start of cooling. The maximum downdraft velocity was $w_{max} = -28.6$ m/s at almost 500 m a.g.l. The value of $U_{storm}/w_{max} \approx 1.4$ observed for this simulation is in close agreement with similar values (1.6) obtained from simulations of Proctor (1989) and Mason et al. (2009). Figure 7 shows the time series of U_{max} and w_{max} which represent, respectively the maximum values of U and W observed anywhere in the domain in the given time steps. All simulated wind speed were normalised with respect to U_{storm}, to allow the analysis of the

ACPD
10, 24345–24370, 2010

maximum speed as compared to with references to U_{storm}. The interpretation of this figure is straightforward if analysed again in terms of the primary and secondary core expansion mentioned earlier. The first "plateau" of U_{max}/U_{storm} depicted between 3 and 6 min is related to the expansion of the primary core, while the second plateau (between 6 and 13 min) appears to be related with the formation of the secondary core with a lower value of $U_{max}/U_{storm} \approx 0.65$. The maximum value of vertical velocity is around 0.75 U_{storm} at elevated region, located 500 m a.g.l. found just before the downdraft impinges the surface. After that it keeps a constant value of 0.60 U_{storm} for almost 10 min before decaying toward the dissipation stage.

The last analysis performed is showed in Fig. 8a, where vertical distribution of the normalized maximum velocity is indicated in a self similar coordinate.

The wind speed profile is normalised with respect to the peak mean wind speed, and height is normalised with respect to the height where the velocity is equal to half its maximum value (Wood et al., 2001). Semi-empirical results based on full scale data (Wood et al., 2001), experimental data (Didden and Ho, 1985; Donaldson and Snedeker, 1971), are reported in Fig. 8b (Kim and Hangan, 2007). The overlapping of Fig. 8a and b portrays a good agreement of the present simulation with experimental data.

6 Conclusions

An isolated and stationary microburst is simulated using a 3-D time-dependent, high resolution Large-Eddy Simulation model with the goal of studying the evolution and the dynamical structure of the microburst. The microburst-producing downdraft is initiated by specifying a simplified cooling source at the top of the boundary in place of a computationally expensive full cloud model. The simulated microburst displayed a vortex ring feature that propagates outward following the leading edge of the cold outflow. The peak horizontal wind speed occurred in association with the expansion of the first core. The simulated time scale for this damaging wind (30 m/s) is of the order of few

ACPD
10, 24345–24370, 2010

min with a spatial scale enclosing a region with 500 m radius around the impact point. The simulated flow reproduces some of the main features of microbursts observed by Doppler Radar, in particular the development of the primary and secondary cores, the formation of the vortex ring at the leading edge of the cold outflow, and finally an accelerating outburst of surface winds. In all of these phases the role of the surface pressure gradient is evidenced and discussed. Additionally, the modelled maximum storm velocity is comparable to that obtained from full-cloud models (Proctor, 1989) and experimental data (Kim and Hangan, 2007).

This evidences the capability of LES in reproducing complex phenomena like a microburst. In fact, LES contains in its basic equations all physical information needed to create the basics mechanism for describing the microburst dynamics: the accelerated downward cold plume, the primary core expansion due to the horizontal pressure gradient and its interaction with environment in order to generate the vortex ring expansion.

These results indicate the potential of LES for utilization in atmospheric phenomena situated below the storm scale and above the microscale, which generally involves high velocities in a short time scale.

Supplementary material related to this article is available online at: http://www.atmos-chem-phys-discuss.net/10/24345/2010/acpd-10-24345-2010-supplement.zip.

Acknowledgements. The authors are gratefully indebted to CNPq (Conselho Nacional de Desenvolvimento Cientifico e Tecnológico, Brasil) and CNR (Consiglio Nazionale delle Ricerche, Itália) for the financial support of this work.

ACPD
10, 24345–24370, 2010

References

Anderson, J. R., Orf, L. G. and Straka, J. M.: A 3-D model system for simulating thunderstorm microburst outflows, Meteor. Atmos. Phys., 49, 125–131, 1992.

Andren, A., Brown, A. R., Graf, J., Mason, J., Moeng, C.-H., Nieuwstadts F. T. M., and Schumann, U.: Large-eddy simulation of a neutrally stratified boundary layer: a comparison of four computer codes, Q. J. R. Meteorol. SOC., 120, 1457–1484, 1994.

ANSYS: ANSYS CFX User's Manual, see: http://www.ansys.com/Products/cfx, 2007.

Atlas, D., Ulbrich, C. W., Willams, C. R.: Physical Origin of a Wet Microburst: Obseervational Theory, J. Atmos. Sci., 61, 1186–1195, 2004.

Bluestein, H. B.: Synoptic-dynamic meteorology in midlatitudes, Oxford University Press, New York, USA, 1993

Didden, N. and Ho, C. M.: Unsteady separation in a boundary layer produced by an impinging jet, J. Fluid Mech., 160, 235–256, 1985.

Donaldson, C. D. and Snedeker, R. S.: A study of free jet impingement, Part 1.: Mean properties of free and impinging jets, J. Fluid Mech., 45, 281–319, 1971.

Elmore, K. L., MacCarthy, J., Frost, W., and Chang, H. P.: A High Resolution Spatial and Temporal Multiple Doppler Analysis for a Microburst and Its Application to Aircraft Flight Simulation, J. Climate Appl. Meteor., 25, 1398–1425, 1986.

FLUENT 6.0 User's Guide: Fluent Inc., Lebanon, December, vol. 1–4, 2001.

Fujita, T. T.: The Downburst- Microburst and Macroburst, Sattellite and Mesometeorology Research Project (SMRP) Research Paper 210, Dept. of Geophysical Sciences, Univ. of Chicago, (NTIS PB-148880), 1985.

Fujita, T.T.: New evidence from April 3–4, 1974 tornadoes, 9th Conf. on severe local storm, 21–23 Oct 1975, Norman. American Meteorological Society, 248-2-55, in preprints, 1975.

Fujita, T. T.: DFW Microburst on August 2, 1985, Univ. of Chicago, SMRP Res. Paper 217, (NTIS No. PB-86-131638), 1986.

Fujita, T. T.: Objectives, operation, and results of Project NIMROD. Preprints, 11th Conf. on Severe Local Storms, KansasCity, MO, Amer. Meteor. Soc., 259–266, 1979.

Hjelmfelt, M. R.: Structure and life cycle of microburst outflows observed in Colorado, J. Climate Appl. Meteor., 27, 900–927, 1988.

Hjelmfelt, M. R., Orville, H. D., Roberts, R. D., Chen, J. P. and Kopp F. J.: Observational and Numerical Study f a Microburst Line-Producing Storm, J. Atmos. Sci., 46, 2731–2743, 1989.

ACPD
10, 24345–24370, 2010

Houze, R. A.: Cloud Dynamics, Academic Press, San Diego, US, 1993.
Joint Airport Weather Studies, "The JAWS Project Operations Summary", JAWS Project Office, NCAR, Boulder, CO, February 1983.
Kim, J., Ho, E., and Hangan, H.: Downburst induced dynamic responses of tall buildings, in: Proceedings of the 10th Americas Conference on Wind Engineering (10 ACWE), Baton Rouge, LA, 2005.
Kim, J. and Hangan, H.: Numerical simulations of impinging jets with application to downbursts, J. Wind. Eng. Ind. Aerod., 95, 279–298, 2007.
Lesieur, M. and Metais, O.: New trends in large-eddy simulation, Annu. Rev. Fluid Mech., 28, 45–82, 1996.
Mason, S. M., Wood, G. S. D. F., and Fletcher D. F.: Numerical simulation of downburst winds, J. Wind Eng. Ind. Aerod., 97, 523–539, 2009.
Mahoney, W. P. and Rodi, A. R: Aircraft measurements on microburst development from hydrometeor evaporation, J. Atmos. Sci., 44, 3037–3051, 1987.
McCarthy, J., Wilson, J. W., and Fujita, T. T.: The Joint Airport Weather Studies Project, Bull. Amer. Meteor. Soc., 63, 15–22, 1982.
Moeng, C.-H.: A Large-Eddy-Simulation Model for the Study of Planetary Boundary-Layer Turbulence, J. Atmos. Sci., 41, 2052–2062, 1984.
Moeng, C.-H. and Sullivan, P. P.: A Comparison of Shear and Buoyancy Driven Planetary Boundary Layer Flows, J. Atmos. Sci. 51, 999–1021, 1994.
Nicholls, M., Pielke R., and Meroney, R.: Large eddy simulation of microburst winds flowing around a building, J. Wind. Eng. Ind. Aerod., 46–47, 229–237, 1993.
Orf, L. G. and Anderson, J. R.: A numerical study of traveling microbursts, Mon. Wea. Rev., 127, 1244–1257, 1999.
Orf, L. G., Anderson, J. R., and Straka, J. M.: A three-dimensional numerical analysis of colliding microburst outflow dynamics, J. Atmos. Sci., 53, 2490–2511, 1996.
Proctor, F. H: Numerical simulations of an isolated microburst, Part II: Sensitivity experiments, J. Atmos. Sci., 46, 2143–2165, 1989.
Sengupta, A., Sarskar, P. P., and Rajagopalan, G.: Numerical and physical simulation of thunderstorm downdraft winds and their effects on buildings, in: Americas Conference on Wind Engineering, 4–6 June 2001, Clemson, SC, 2001.
Srivastava, R. C.: A simple model of evaporatively driven downdrafts: Application to microburst downdraft, J. Atmos. Sci., 42, 1004–1023, 1985.

ACPD
10, 24345–24370, 2010

Srivastava, R. C.: A model of intense downdrafts driven by melting and evaporation of precipitation, J. Atmos. Sci., 44, 1752– 1773, 1987.

Straka, J. M. and Anderson, J. R.: The numerical simulations of microburst-producing thunderstorms: Some results from storms observed during the COHMEX experiment, J. Atmos. Sci., 50, 1329–1348, 1993.

Straka, J. M. and T. R. Mansell, T.R.: A bulk microphysics parameterization with multiple ice precipitating categories, J. Appl. Meteor., 44, 445–466, 2005.

Sullivan, P. P., McWilliams, J. C., and Moeng, C.-H.: A subgrid-scale model for large-eddy simulation of planetary boundary-layer flows, Bound.-Lay. Meteorol., 71, 247–276, 1994.

Wakimoto, R. M.: Forecasting microburst activity over the High Plains, Mon. Wea. Rev., 113, 1131–1143, 1985.

Wakimoto, R. M. and Bringi, V. N.: Dual-polarization observations of microbursts associated with intense convection: The 20 July storm during the MIST project, Mon. Wea. Rev.,116, 1521–1539, 1988.

Wakimoto, R. M., Kessinger, C. J., and Kingsmill, D. E.: Kinematic, thermodynamic, and visual structure of low-reflectivity microbursts, Mon. Wea. Rev., 122, 72–92, 1994.

Wood, G. S., Kwok, K. C. S., Motteram, N. A., and Fletcher, D. F.: Physical and numerical modelling of thunderstorm downbursts, J. Wind Eng. Ind. Aerod., 89, 535–552, 2001.

Wolfson, M. M., Distefano, J. T., and Forman, B. E.: The FLOWS Automatic Weather Station Network in Operation. MIT, Lincon Laboratory Project Report ATC-134, FAA Report DOT-FAA-PM-85/27, 1986.

ACPD

10, 24345–24370, 2010

Table 1. Position (x_f,y_f,z_f) and extension (Mx,My,My) of the forcing function and its Cooling Rate.

(x_f,y_f,z_f)	(Mx,My,Mz)	CR
km	km	Ks^{-1}
(5, 5, 2)	(2, 2, 1.8)	0.08

ACPD
10, 24345–24370, 2010

Table 2. Internal parameters of the LES domain.

(Nx,Ny,Nz)	(Lx,Ly,Lz)	Q_*	(Ug,Vg)	$(z_i)_0$
		($ms\,K^{-1}$)	ms^{-1}	m
128^3	(10, 10, 2)	0.25	(3.0, 0)	1500

ACPD
10, 24345–24370, 2010

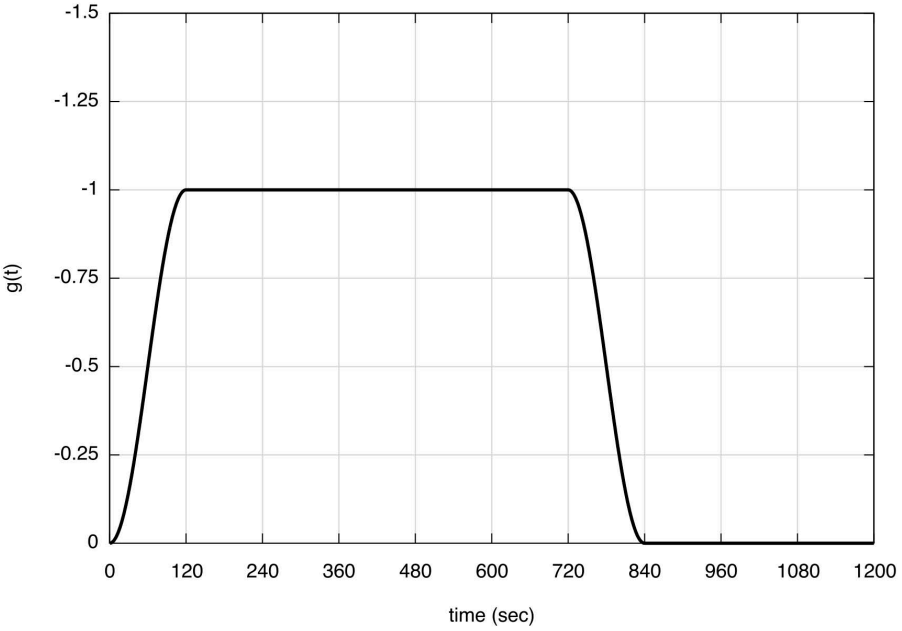

Fig. 1. Temporal modulation of the maximum intensity of the cooling function.

ACPD
10, 24345–24370, 2010

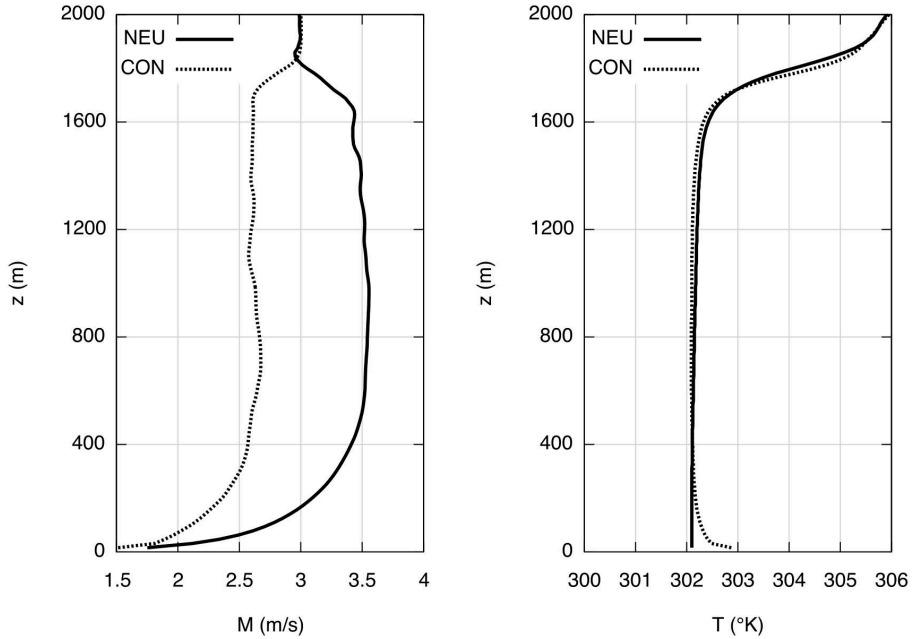

Fig. 2. Magnitude of the mean wind speed profiles (left) and potential temperature (right) in the convective (dotted line) and neutral (continuous line) PBL.

ACPD
10, 24345–24370, 2010

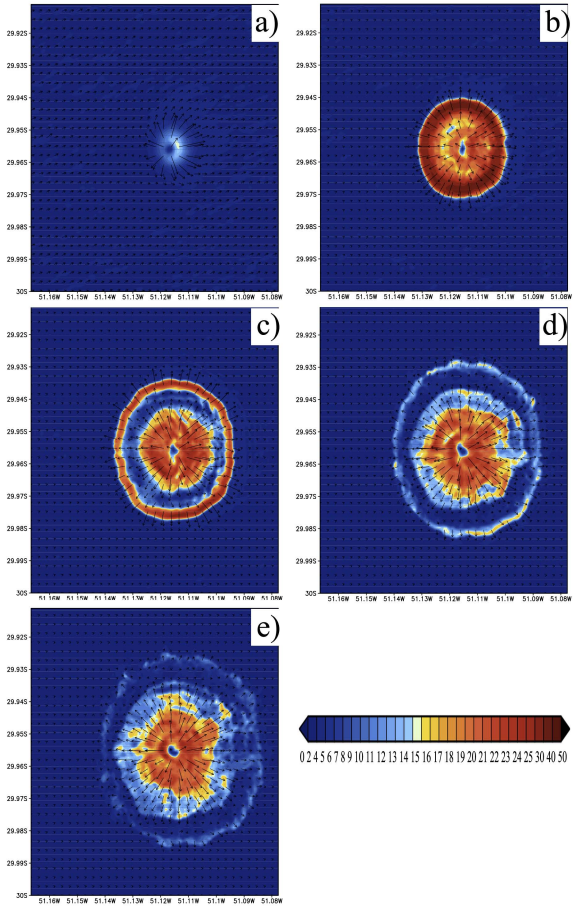

Fig. 3. Magnitude of surface winds at the first vertical level of the LES grid, respectively **(a)** 3, **(b)** 5, **(c)** 6, **(d)** 8 and **(e)** 10 min after the start of cooling.

ACPD
10, 24345–24370, 2010

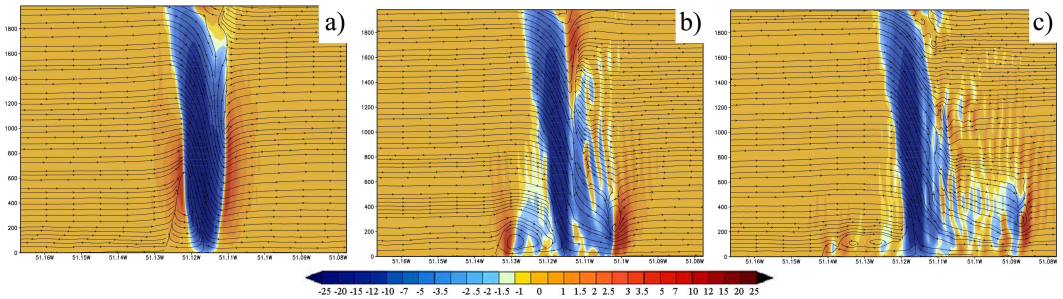

Fig. 4. Vertical velocity in a (x–z) section of the LES domain, respectively **(a)** 3, **(b)** 5 and **(c)** 8 min after the start of cooling.

ACPD
10, 24345–24370, 2010

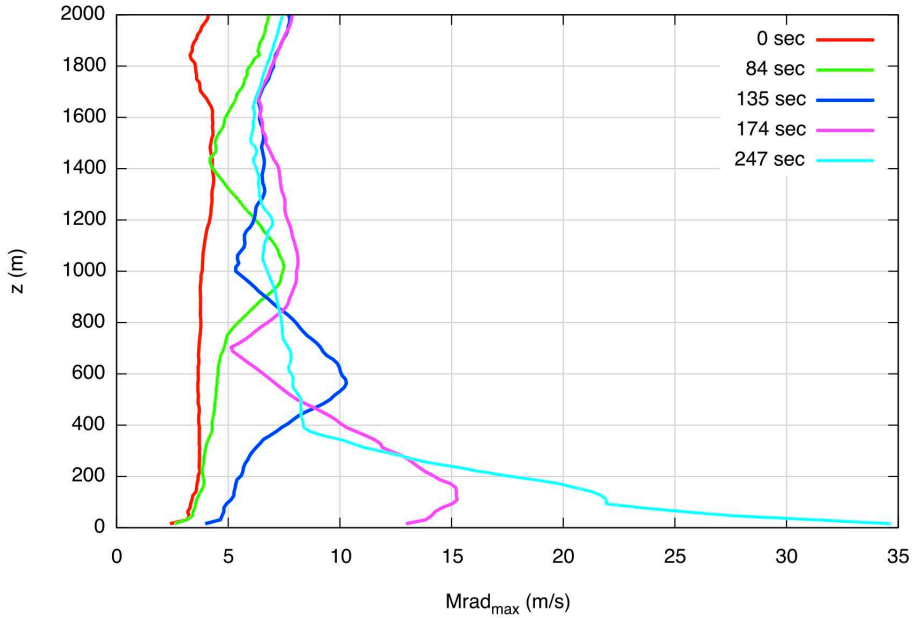

Fig. 5. Vertical distribution of the maximum of the radial velocity. Times are taken after the start of cooling (red line).

ACPD
10, 24345–24370, 2010

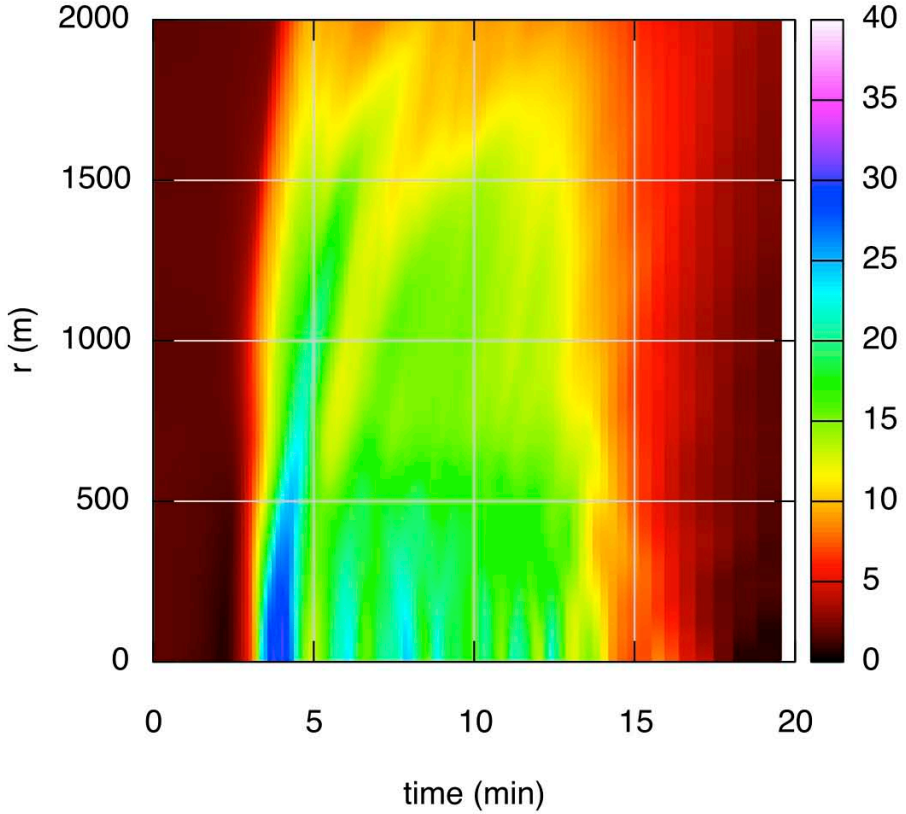

Fig. 6. Time-radial distance plot of the wind field magnitude at the first vertical level of the LES domain.

ACPD
10, 24345–24370, 2010

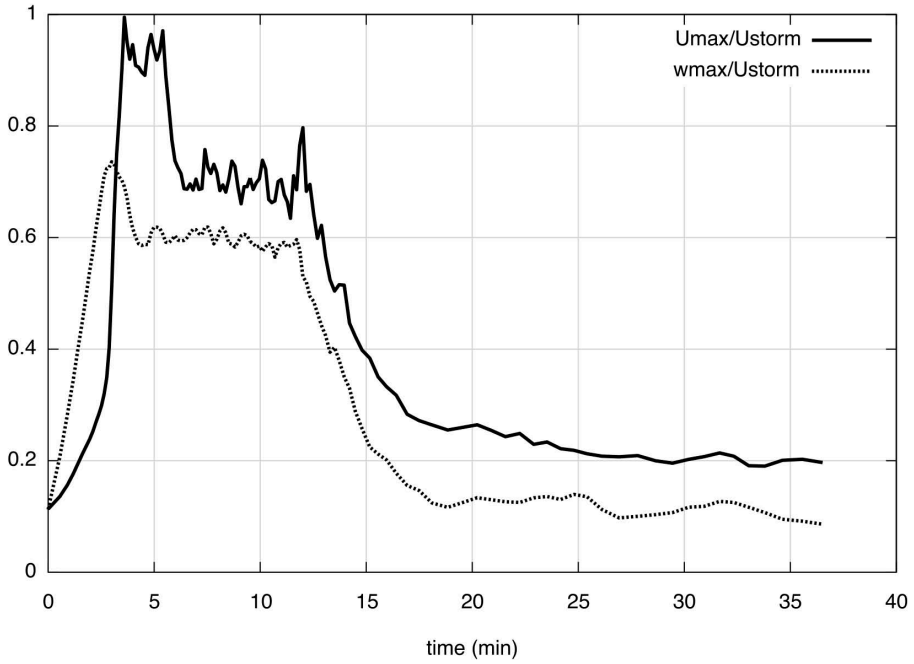

Fig. 7. Temporal variation of the normalized maximum storm event wind speed (U_{max}) and the maximum downdraft velocity (w_{max}).

ACPD
10, 24345–24370, 2010

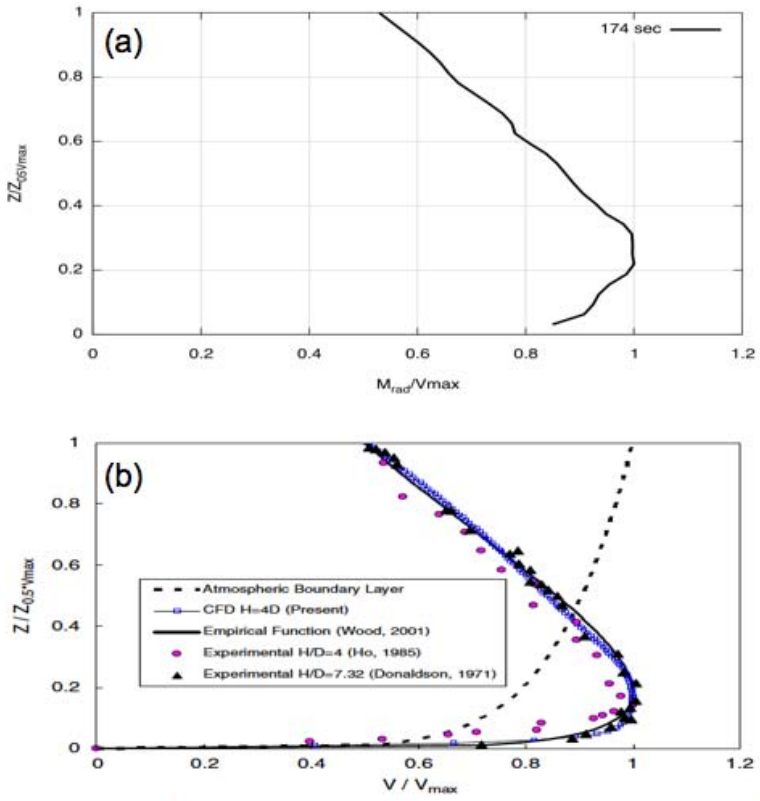

Fig. 8. Vertical distribution of the normalized maximum velocity in self-similar coordinate, **(a)** present simulation, **(b)** semi-empirical results (reprinted with permission of Journal of Wind Engineering and Industrial Aerodynamics).

ACPD
10, 24345–24370, 2010